



## RESEARCH ARTICLE

10.1029/2022JG007365

### Key Points:

- Ebullition and degassing accounted for 93% of methane emissions, 66% of ebullition variability was explained by environmental parameters
- The free gas stored in the sediment was variable in space and time and can affect methane dynamics in aquatic systems
- The sediment matrix can store the cumulative methane production of several days and can supply the ebullition flux for weeks

### Supporting Information:

Supporting Information may be found in the online version of this article.

### Correspondence to:

L. Marcon,  
[ledi.marcon@gmail.com](mailto:ledi.marcon@gmail.com)

### Citation:

Marcon, L., Schwarz, M., Backes, L., Offermann, M., Schreiber, F., Hilgert, S., et al. (2023). Linking sediment gas storage to the methane dynamics in a shallow freshwater reservoir. *Journal of Geophysical Research: Biogeosciences*, 128, e2022JG007365. <https://doi.org/10.1029/2022JG007365>

Received 23 DEC 2022

Accepted 20 SEP 2023

### Author Contributions:

**Conceptualization:** Lediane Marcon, Laura Backes, Mara Offermann, Klajdi Sotiri, Christian Jokiel, Andreas Lorke

**Data curation:** Lediane Marcon, Laura Backes, Mara Offermann

**Formal analysis:** Lediane Marcon, Laura Backes, Andreas Lorke


**Funding acquisition:** Christian Jokiel, Andreas Lorke

**Investigation:** Lediane Marcon, Michael Schwarz, Laura Backes, Mara Offermann, Felix Schreiber, Stephan Hilgert, Andreas Lorke

© 2023. The Authors.

This is an open access article under the terms of the [Creative Commons Attribution License](https://creativecommons.org/licenses/by/4.0/), which permits use, distribution and reproduction in any medium, provided the original work is properly cited.

# Linking Sediment Gas Storage to the Methane Dynamics in a Shallow Freshwater Reservoir

Lediane Marcon<sup>1,2</sup> , Michael Schwarz<sup>1</sup>, Laura Backes<sup>3</sup>, Mara Offermann<sup>4</sup>, Felix Schreiber<sup>3</sup>, Stephan Hilgert<sup>5</sup>, Klajdi Sotiri<sup>5</sup>, Christian Jokiel<sup>4</sup>, and Andreas Lorke<sup>1</sup> 

<sup>1</sup>Institute for Environmental Sciences, RPTU Kaiserslautern-Landau, Landau, Germany, <sup>2</sup>Post-graduate Program on Water Resources and Environmental Engineering (PPGERHA), Federal University of Paraná, Curitiba, Brazil, <sup>3</sup>D-Sediment GmbH, Werne, Germany, <sup>4</sup>Faculty of Civil and Environmental Engineering, Institute for Building Materials, Geotechnics, Traffic and Water (IBGVW), University of Applied Science Cologne, Köln, Germany, <sup>5</sup>Department of Aquatic Environmental Engineering, Institute for Water and River Basin Management, Karlsruhe Institute of Technology, Karlsruhe, Germany

**Abstract** Freshwater reservoirs are globally relevant sources of the greenhouse gas methane. Organic matter rich sediments are hot spots of methane production and can store large amounts of methane dissolved in porewater and as free gas. Yet, in situ data on the gas storage as free gas (bubbles) in freshwater sediments are scarce. Here, an acoustic approach was tested and used to map the gas content in the sediment of a shallow temperate reservoir. The sediment gas storage was linked to the methane budget obtained from almost 2 years of in situ monitoring. The emission fluxes were dominated by ebullition and degassing at the reservoir outlet, which combined accounted for 93% of the total methane emissions. 66% of the ebullition variability was explained by a combination of environmental parameters. Mappings of sediment gas content using echo sounder surveys revealed the accumulation of free gas in regions of elevated sediment deposition. Temporally, the gas storage in the sediment was related to methane emissions, in which a period of intensified emissions resulted in a reduction of sediment gas storage. The sediment could store an equivalent of 4 to 13 days of accumulated potential methane production, which could supply the mean ebullition flux for more than 2 months. We suggest that sediment gas storage plays an important role in buffering and modulating methane emissions in aquatic systems and need to be accounted for in process-based models.

**Plain Language Summary** Methane is a potent greenhouse gas, and it is naturally produced in sediments of freshwater aquatic ecosystems. In the sediment, methane is found in dissolved form in the porewater, or as free gas (bubbles). It can be emitted to the atmosphere as a diffusive flux across the air-water interface, by ebullition flux (gas bubbles rising from the sediment), or by degassing as the water passes through turbines or over spillways at the reservoir outflow. Here, we estimated the gas content in the sediment matrix of a shallow freshwater reservoir based on acoustic (echo-sounder) measurements. We found that the amount of gas stored in the sediment is linked to variations in methane emissions and vice versa. At our study site, ebullition and degassing accounted for 93% of the methane emissions from the reservoir. We suggest that the sediment storage can affect the fate of methane produced in the sediments and the temporal dynamics of its emission to the atmosphere, which is not accounted for in existing mechanistic models.

## 1. Introduction

Freshwater aquatic ecosystems are a relevant source of atmospheric methane (CH<sub>4</sub>), an important greenhouse gas contributing 16% to the effective radiative forcing (IPCC, 2021). Manmade reservoirs are estimated to emit 18–24 TgCH<sub>4</sub> per year to the atmosphere, corresponding to 2.2%–3% of anthropogenic sources (Deemer et al., 2016; Rosentreter et al., 2021). Nevertheless, the magnitude of methane emissions from reservoirs as well as from other inland waters (i.e., rivers, lakes, and wetlands) is still highly uncertain (Saunio et al., 2020).

The damming of rivers is often associated with a change from lotic to lentic ecosystem characteristics, including changes in sediment retention, flow velocity, as well as thermal and chemical conditions (Maavara et al., 2017). Combined they favor the production of CH<sub>4</sub> and its emission to the atmosphere (Maavara et al., 2020). The spatial and temporal dynamics of CH<sub>4</sub> emission from these aquatic systems have been increasingly investigated with the aim to understand and to identify the governing processes. Improved mechanistic understanding is key for upscaling of flux measurements in space and time, for making predictions of ongoing and future changes, and to develop mitigation strategies together with optimized management strategies.

**Methodology:** Lediane Marcon, Michael Schwarz, Laura Backes, Mara Offermann, Stephan Hilgert, Klajdi Sotiri, Andreas Lorke

**Project Administration:** Christian Jokiel, Andreas Lorke

**Supervision:** Andreas Lorke

**Visualization:** Lediane Marcon

**Writing – original draft:** Lediane Marcon, Andreas Lorke

**Writing – review & editing:** Lediane Marcon, Michael Schwarz, Mara Offermann, Felix Schreiber, Stephan Hilgert, Klajdi Sotiri, Andreas Lorke

In freshwater reservoirs, CH<sub>4</sub> is mostly formed during the anaerobic degradation of organic matter (Bastviken, 2009; Smith et al., 2003). Deposition zones of sediments being rich in organic matter are hotspots of CH<sub>4</sub> production (DelSontro et al., 2011; Hilgert et al., 2019; Maeck et al., 2013), while the fate of the produced CH<sub>4</sub> is determined by the prevailing environmental conditions. In the sediment CH<sub>4</sub> can be oxidized by bacteria, which can consume up to 95% of the methane produced (Bastviken, 2009); CH<sub>4</sub> can be transported into the surface water by diffusion; If the net CH<sub>4</sub> production in the sediment results in dissolved gas pressure exceeding the ambient hydrostatic pressure, gas voids can form, from which events of bubble release (ebullition flux) can transport CH<sub>4</sub> out of the sediment matrix. In shallow reservoirs, ebullition fluxes, which bypass CH<sub>4</sub> oxidation, can dominate the emissions (Bastviken et al., 2004).

The bottom sediment plays an important role for CH<sub>4</sub> dynamics in water reservoirs. In addition to its influence on the production and transport, the sediment matrix can store CH<sub>4</sub> dissolved in the pore water or as free gas. The gas void fraction in the sediment has been reported in the range from <1% (Uzhansky et al., 2020) for in situ measurements up to 18% under laboratory conditions (Liu et al., 2016). The sediment storage capacity for free gas depends on ambient conditions, such as temperature and pressure, and on the mechanical properties of the sediment (Liu et al., 2018, 2019).

Recent models for CH<sub>4</sub> emissions from wetland have introduced gas storage for predicting ebullition dynamics (Peltola et al., 2018). Yet data on gas storage and its spatial and temporal variability in other inland waters are scarce. Katsnelson et al. (2017) estimated the gas content in the sediment of lake Kinneret based on measurements of the reflection coefficient of low-frequency sound and found that spatial patterns of sediment reflectance coincided with the distribution of organic matter. At the same lake, Uzhansky et al. (2020) showed that the gas content in the sediment was lower during periods of higher water level. Martinez and Anderson (2013) measured the areal sediment gas content in a eutrophic reservoir and identified it as a driver of ebullition. In a follow-up study, Anderson and Martinez (2015) proposed an empirical calibration to estimate the areal gas content based on the maximum acoustic backscatter observed in the bottom echo of high-frequency echo-sounders. This calibration curve was also applied to estimate gas content in another aquatic system (Marcon, Sotiri, et al., 2022).

In this study, we estimated the free gas stored in the sediment of a freshwater reservoir in Germany with the use of an echo-sounder and the method proposed by Anderson and Martinez (2015), which we validated using in situ measurements. For the first time, we relate the sediment gas content to the reservoir CH<sub>4</sub> budget, which we derived from extensive field measurements of fluxes and potential production rates. Our analysis follows three main objectives: (a) to establish a methane budget for a shallow freshwater reservoir; (b) to evaluate the spatio-temporal dynamics of methane emissions from the system; and (c) to link the spatial and temporal dynamics of sediment gas storage to the methane budget.

## 2. Materials and Methods

### 2.1. Study Site and Sampling Overview

This study was conducted in the Wupper-Vorsperre, which is the main pre-dam of the Wupper reservoir. The reservoir is located in the western part of Germany (coordinates 51.16°N and 7.33°E). It was built in 1976 primarily for flood control, but it is also used for energy generation, with an installed capacity of 1.25 MW. Reservoir pre-dams, also known as check dams, are often built for controlling sediment input (Morris, 2020) and water quality (Paul, 2003) in the main reservoir. The Wupper pre-dam (hereafter also referred as reservoir) in which our sampling was conducted, has a surface area of 150,000 m<sup>2</sup>, an average depth of 2 m, and a maximum depth of 5.5 m close to the dam. It has an elongated, curved shape with approximately 2.4 km length from the inflow to the dam and an average width of 77 m. The bathymetry clearly shows the location of the talweg of the former river course, and a preference of sediment accumulation at the inner curves of the reservoir, similar to sediment deposition patterns typically described in rivers bends (Wetzel, 2001), as well as in the shallow upstream regions near to the inflow (Figure 1).

The main inflow to the reservoir is the Wupper River. The river discharge is monitored by a gauging station approximate 1.5 km upstream of the reservoir entrance (operated by Wupperverband). From March 2020 to December 2021, the average daily inflow discharge was  $3.3 \pm 4.0 \text{ m}^3 \text{ s}^{-1}$  (average  $\pm$  standard deviation), nevertheless peak discharges exceeding  $30 \text{ m}^3 \text{ s}^{-1}$  were recorded in mid March 2020 and mid July 2021 (see Figure S1 in Supporting Information S1). In July 2021, a major flood event occurred in the region, causing a significant

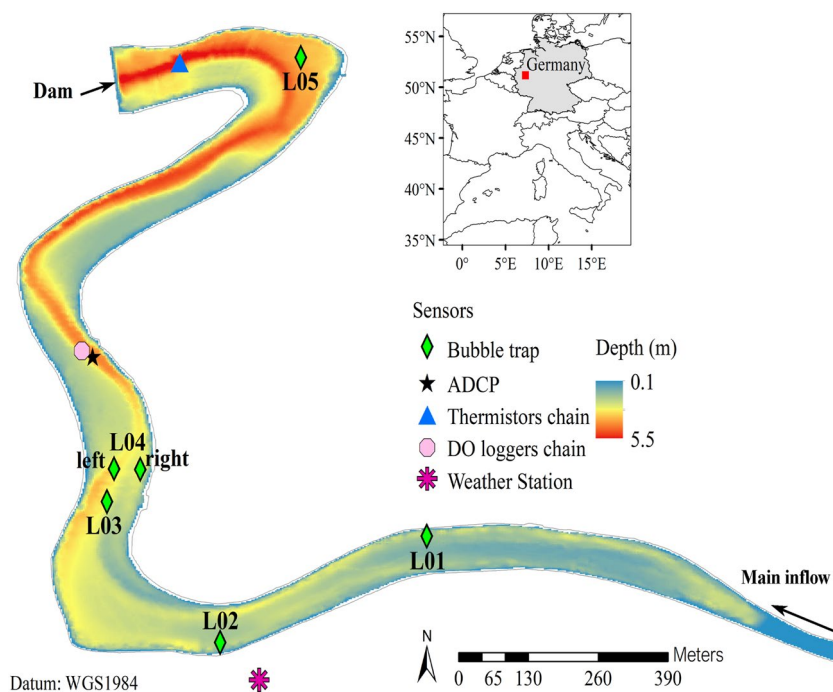


**Figure 1.** Map of the study site, Wupper pre-dam, located in the western region of Germany (see inset map). The location of the monitoring sites is marked by symbols indicating the different measuring device deployed and the color shows the reservoir bathymetry, see Figure legend.

increase in the water level overflowing the reservoir banks. A wastewater treatment plant (WTP) is located near the upper part of the reservoir, with an effluent discharge location upstream of the monitoring site L02.

The monitoring in the reservoir was conducted from March 2020 to November 2021 with a combination of continuous sensor measurements and monthly field campaigns. The measurements comprised methane fluxes and concentrations, and relevant environmental parameters detailed on the following sections. Data gaps in continuous measurements and in monthly samplings were caused by sensor failure, logistic limitations, or weather and hydrological conditions, such as floods.

## 2.2. Methane Fluxes

We measured  $\text{CH}_4$  fluxes by ebullition, diffusive gas exchange at the water surface, advective fluxes with inflows and outflows, degassing at the outflow spillway, and ecosystem  $\text{CH}_4$  oxidation rates. The measurements and respective flux calculation are outlined below, and more detailed information are provided in Text S1 in the Supporting Information S1.

Gas ebullition was continuously monitored using bubble traps with logging capabilities, which were deployed at five monitoring locations (from L01 to L05, see Figure 1). Detailed description of the devices and ebullition calculation is provided in Supporting Information (Text S1 in the Supporting Information S1). Depending on location, valid ebullition fluxes were recorded for a total of 85 days (at L05) up to 362 days (at L03) for the monitoring period from 18 March 2020 to 28 November 2021. At each monitoring site, gas bubbles from the sediment were monthly captured and analyzed for the methane fraction within the gas samples, which was used for the calculation of the  $\text{CH}_4$  ebullition fluxes. Daily  $\text{CH}_4$  ebullition fluxes were obtained for each monitoring site. The daily fluxes were then used to obtain the mean and median fluxes at each monitoring site to evaluate its spatial distribution. In addition, daily values of spatially averaged fluxes (average of all monitoring sites) were used to analyze the temporal dynamics of reservoir-wide ebullition fluxes.

The diffusive  $\text{CH}_4$  flux at the air-water interface was estimated for 14 months from monthly measured dissolved  $\text{CH}_4$  concentrations in the surface water and by applying the thin boundary layer method. The  $\text{CH}_4$  diffusive flux crossing the air-water interface was calculated from the difference between the dissolved concentration and the

atmospheric equilibrium concentration at in situ water temperature, and the gas transfer velocity, which was estimated from wind speed (Liss & Slater, 1974).

The water outflow from the pre-dam to the main reservoir is through a spillway overflow at the dam and from two bottom outlets controlled by gates. The passage of water over the spillway enhances the release of the dissolved methane to the air (degassing flux). The degassing flux was calculated for 10 months during the monitoring period as proposed by Goldenfum (2010), as the product of the difference in dissolved CH<sub>4</sub> concentration upstream and downstream the dam, and the water discharge. Despite being rather a point source, the degassing flux is normalized by the reservoir surface area to facilitate comparison with other fluxes. The difference between the dissolved CH<sub>4</sub> exported and imported by water leaving and entering the reservoir was used to calculate a net advective CH<sub>4</sub> flux, which was available for 8 months and also normalized by reservoir surface area.

Lastly the CH<sub>4</sub> oxidation rate was estimated as proposed by Sawakuchi et al. (2016). In summary, the fraction of CH<sub>4</sub> oxidized was calculated by applying the Rayleigh isotopic fractionation model (Langrangian, closed system model) using measurements of the isotopic ratios of methane carbon ( $\delta^{13}\text{C-CH}_4$ ) in bubbles stirred from the sediment and in dissolved CH<sub>4</sub> in the surface water. The underlying assumption of this method is that the diffusive CH<sub>4</sub> flux at the water-air interface represents the total dissolved CH<sub>4</sub> that escaped oxidation, while the input of methane into the water column is the sum of the diffusive flux at the water surface and the fraction of the input that is oxidized (Sawakuchi et al., 2016). For further details, see Text S1 in Supporting Information S1. Oxidation rates were estimated based on monthly measurements for 13 months of the monitoring period.

### 2.3. Sediment Sampling

Sediment cores with 6 cm diameter were sampled at all sites (L01 to L05) in May, July, and September 2020 using a gravity corer (Uwitec). The length of the sampled sediment cores varied from ~32 to ~42 cm. After retrieval, the sediment cores were transported to the laboratory and kept at a temperature of ~4°C until analysis. In the laboratory, the sediment cores were analyzed for dissolved CH<sub>4</sub> concentration in the porewater, potential methane production (PMP), and organic matter content. An extended explanation of the sampling procedure is provided in the Supporting Information (Text S2 in Supporting Information S1).

Sediment porewater was extracted from sediment layers (3 cm vertical spacing at the top 15 cm and at 10 cm spacing for the remaining of the core) using Rhizon tubes inserted into pre-drilled holes, as described by Wilkinson et al. (2019). The porewater was transferred to pre-evacuated glass vials, and the dissolved CH<sub>4</sub> concentration in porewater was calculated from the CH<sub>4</sub> headspace concentration measured in the vials. The sediment cores were then sliced into 3–10 cm layers in a nitrogen flushed glove box, transferred to 120 ml nitrogen flushed serum bottles, and incubated under dark conditions at a constant temperature of 20°C for the estimation of PMP rates in the sediment. The volumetric PMP rates from the individual incubated sediment layers of the top 30 cm of each core were then vertically integrated to obtain the potential methane flux at the sediment water interface (PSWI) in units of mgCH<sub>4</sub> m<sup>-2</sup> d<sup>-1</sup>, which was adjusted to in situ sediment temperature (Wilkinson et al., 2015, 2019).

The remaining sediment from each core layer was transferred to falcon tubes, freeze-dried, and stored for measurement of organic matter content. The organic matter content in the sediment was estimated from Loss on Ignition (LOI). In addition to the LOI, the carbon and nitrogen content in the sediment samples were estimated using a CHNS (Carbon-Hydrogen-Nitrogen-Sulfur) elemental analyzer (Vario MicroCUBE, Germany).

### 2.4. Echo-Sounding and Estimation of Sediment Gas Content

An initial echo-sounding survey for obtaining the reservoir bathymetry was conducted in May 2021 with a GSD 26 echo-sounder (Garmin) and a Airmar CM599LH transducer with a frequency of 180–210 kHz. Two additional surveys with a dual frequency (38 and 200 kHz) single beam echo-sounder (EA400, Kongsberg Inc. 2006) were conducted for estimating the amount of free gas (bubbles) in the sediment (sediment gas content). The first survey was conducted on July 1st of 2020 and covered the entire pre-dam. The second survey was conducted on June 11th of 2021 but restricted to the upstream region of the pre-dam (from monitoring site L04 towards the upstream site L01, see map at Figure 1 for the monitoring locations) due to logistic reasons.

The areal gas content in the sediment was estimated from the EA400 echo-sounder data following Marcon, Sotiri, et al. (2022). The 200 kHz measurements were processed using the Sonar5-Pro software (Lindem Data

Acquisition, Oslo, Norway), in which the magnitude of the maximum acoustic backscatter near the sediment surface is exported together with its geographic coordinates for each ping (sound pulse). A spatial grid of 5 m by 5 m was created for the pre-dam and the average maximum backscatter was calculated with the available measurements for each grid cell. Anderson and Martinez (2015), proposed an empirical relationship between the areal gas content in the sediment (in  $L\ m^{-2}$ ) and the maximum backscatter strength at a frequency of 200 kHz. We validated and applied this relationship for mapping the gas content in the sediment of the reservoir.

The calibration equation from Anderson and Martinez (2015) was tested with four in situ measurements in a cross-section of the reservoir with water depth varying from 2 to 3.5 m (see Figures S2 and S3 in Supporting Information S1). The measurements were conducted on June 17th of 2021. A rope fixed to trees at both banks of the cross-section was used to maintain the boat at a fixed position during the measurements. At each location, stationary echo-sounder measurements with the EA400 were conducted for 1 min. After these measurements, a self-made device was used to capture the gas stored in the sediment by inserting an aluminum cylinder with an inner moving mesh (24.5 cm diameter and 35 cm length) into the sediment. The upper 30–39 cm of the sediment were mechanically disturbed using the vertically moving mesh, and the volume of gas that was released during the disturbance was measured. A detailed description of the cylinder is provided in the Supporting Information (Text S3 in Supporting Information S1). A sediment depth of 30 cm was adopted to calculate the volumetric gas fraction from the estimated gas content. This sediment thickness was selected based on the vertical profiles of potential methane production obtained from incubated sediment cores, as we expect that the largest part of gas content in the sediment matrix is from the top productive sediment layer.

## 2.5. Auxiliary Measurements

Temperature in the surface sediment was recorded at locations L01, L03, and L05 in 4 hr time intervals by temperature loggers (HOBO® loggers). The loggers were attached to the lower side of anchor weights used for bubble trap deployments. Water temperature was monitored at depth increments of 0.5 m by thermistors (RBR TR-1050) at 1 min time intervals. The thermistor chain was deployed downstream of location L05, closer to the dam (Figure 1). Vertical thermal stratification was assessed in terms of the relative water column stability (RWCS) also referred to as the relative thermal resistance to mixing (Welch & Naczk, 1992):

$$RWCS = \frac{\rho_{\text{bottom}} - \rho_{\text{surface}}}{\rho_{4^{\circ}C} - \rho_{5^{\circ}C}},$$

in which  $\rho_{\text{bottom}}$  and  $\rho_{\text{surface}}$  are the water densities at the bottom and at the surface respectively,  $\rho_{4^{\circ}C}$  and  $\rho_{5^{\circ}C}$  are the water densities at temperatures of 4°C and 5°C. The water density as a function of temperature was calculated using the UNESCO equation (Fischer et al., 1979). For  $RWCS > 56.5$ , the reservoir is considered as stratified,  $RWCS < 16.3$  indicates a mixed water column, and  $16.3 < RWCS < 56.5$  indicates partial stratification (Branco et al., 2009; Gerardo-Nieto et al., 2017).

Dissolved oxygen (DO) concentration was continuously monitored near the bottom (0.3 m above the sediment) and near the water surface (0.5 m depth). The oxygen loggers (MiniDot, PME) were deployed near the monitoring site L04 and recorded at 5 min intervals. Near the oxygen loggers, an upward-looking Acoustic Doppler Current Profiler (ADCP, Nortek AS-Signature 1000) was deployed from August 24th of 2020 to July 13th of 2021 at the bottom for recording vertical profiles of flow velocity (from approximately 0.6 m above the sediment to approximately 0.5 m below the water surface). The ADCP recorded vertical profiles of all three velocity components with a vertical resolution of 0.2 m and a temporal resolution of 5 min. In addition, the ADCP also recorded bottom water temperature and pressure.

Time series of discharge and atmospheric pressure were available for the sampling period from stations maintained by the reservoir operator Wupperversband. Inflow discharge was recorded at 20 s time interval by a gauging station in the Wupper River, approximately 1.5 km upstream the reservoir. Atmospheric pressure was measured at 30 min time intervals by a weather station located 2 km from the reservoir. In addition, a weather station (MWS 9-5, Reinhardt System und Messelectronic GmbH) was installed next to the reservoir (approx. 70 m from monitoring location L02, see Figure 1 for location) for recording meteorological data at 3 m height above ground. Air temperature, barometric pressure, wind direction and velocity, and solar radiation are available from August 2020 to May 2021 with 15 min resolution.

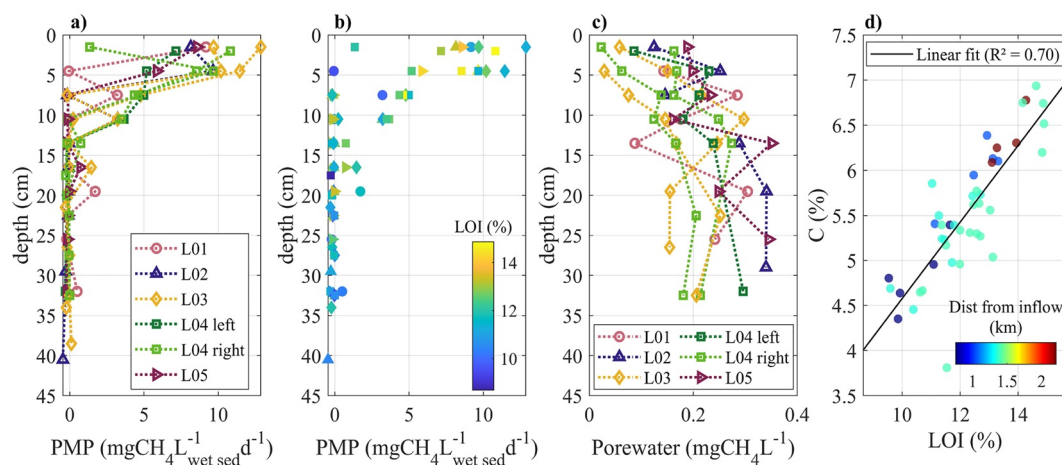


**Figure 2.** (a) Vertical profiles of potential methane production (PMP) in the sediment at the different monitoring locations (see legend for explanation of symbols and colors). (b) Vertical profile of PMP combined with the Loss on Ignition (LOI) for the sediment samples. Symbols represent the monitoring locations, see legend in (a), and the color shows the LOI range. (c) Vertical profiles of dissolved methane concentration in the porewater in the sediment cores. (d) Comparison of carbon content (c) and LOI for all sediment samples. The symbol color scales with the distance of the sampling location from the river inflow and the solid line is the linear fit  $C = 0.425 \text{ LOI} + 0.326$ .

### 3. Results

#### 3.1. Reservoir Conditions

The current velocities in the reservoir were correlated with inflow discharge (Spearman correlation  $r_s = 0.82$ ) with a mean value of  $2.9 \pm 2.1 \text{ cm s}^{-1}$  (average  $\pm$  standard deviation). No significant correlation was found between wind velocity and current, nevertheless, periods were observed in which increased variability in the flow velocity were observed at high wind speed (see Figure S1 in Supporting Information S1).

The DO concentration near the bottom was found to be similar to the concentration recorded at the water surface for most of the monitoring period. For 76% of the time, the difference between surface and bottom DO was smaller than  $1 \text{ mg L}^{-1}$ , except from February 2021 to July 2021, when the DO concentration at the bottom decreased to  $0.22 \text{ mg L}^{-1}$  (Figure S1 in Supporting Information S1). On average, the DO concentrations were  $8.7 \pm 1.7 \text{ mg L}^{-1}$  and  $9.6 \pm 1.2 \text{ mg L}^{-1}$  at the bottom and surface, respectively. This weak vertical stratification or lack thereof was also observed for the vertical distribution of flow velocity and water temperature and can be attributed to the shallow depth of the reservoir.

Top sediment temperature from three different locations along the reservoir was similar and indicated a nearly homogeneous longitudinal sediment temperature distribution (Figure S1 in Supporting Information S1). The difference between daily mean sediment temperature at the shallowest (L01) and at the deepest (L05) sampling sites was smaller than  $1^\circ\text{C}$  during 88% of the time. The maximum sediment temperature of  $17.4^\circ\text{C}$  was recorded at the deepest monitoring site (location L05) in August 2020, and the lowest temperature of  $1.6^\circ\text{C}$  was recorded in February 2021 at the shallowest sampling location (L01). The temporal dynamics of sediment temperature was similar to that in the overlying water column. The relative water column stability indicates that the reservoir was thermally stratified (RWCS  $>56.5$ ) for 8% of the monitored period, particularly during the warmer months. For 59% of the time, the reservoir was fully mixed (RWCS  $<16.3$ ), and in the remaining time, the reservoir was classified as partially stratified (Figure S1 in Supporting Information S1).

#### 3.2. Methane in the Sediment: Vertical Profiles and Spatial Distribution of Gas Content

The PMP from incubated sediment samples was generally higher in the top sediment layers and decreased towards deeper sediment layers. Most of the methane production occurred within the top 20 cm layer (Figure 2a). In deeper, less productive sediment layers, the incubations resulted in near-zero and sometimes slightly negative production rates. Although, the sediment preparation and incubation were conducted in a sealed, nitrogen-flushed glovebox, any remaining oxygen concentration in the incubation glass vials may have influenced the estimates,

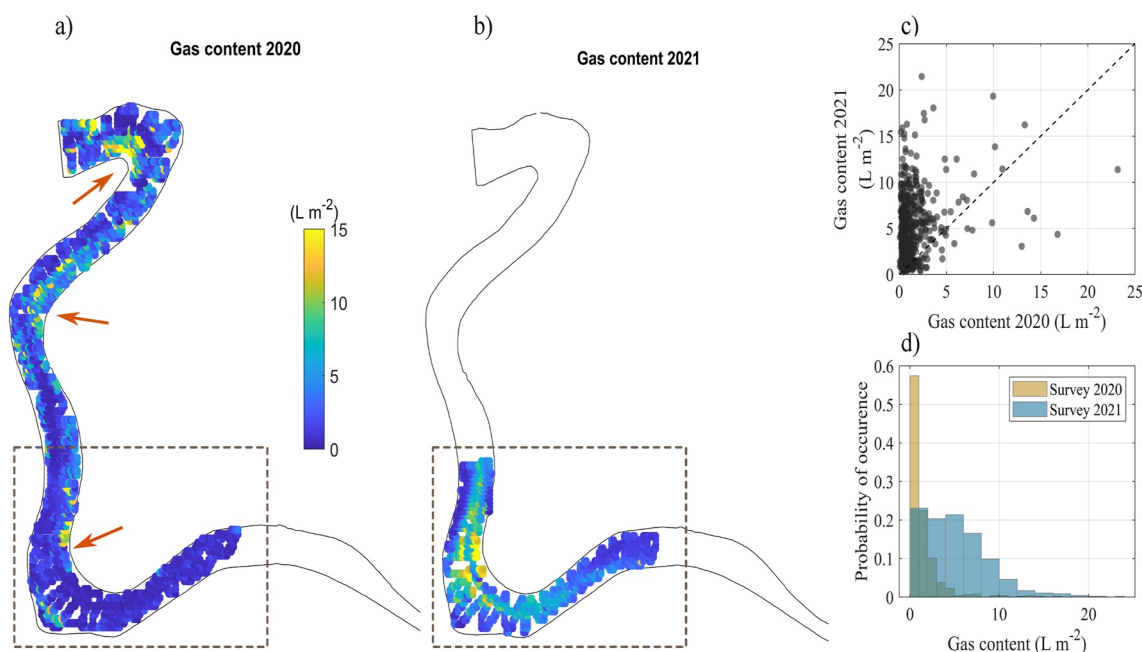


**Figure 3.** Sediment gas content estimated from echo-sounder surveys conducted in (a) 11 June 2020 and (b) 1 July 2021, respectively. The solid black line shows the outline of the reservoirs and colored symbols show the mean gas content within 5 m by 5 m grid cells along the tracks of echo-sounding surveys. The red arrows in (a) point to regions of high gas accumulation. The dashed box shows the region where measurements are available from both years. (c) Scatter plot of gas content measurements in individual grid cells made in both years with the dashed black line indicating a 1:1 relationship. (d) Probability of occurrence histograms of estimated gas content in the sediment, with colors indicating the year of measurement.

particularly for low production rates. Furthermore, the closed-loop measurements in the gas analyzer, which have been reported to have an uncertainty range of 6%–10% (Wilkinson et al., 2018), could also have contributed to a high relative uncertainty in low production rates, including also negative values. Longitudinally, slight variations were observed in PMP with higher production rates on the reservoir stretch between sites L02 and L04.

Loss on Ignition (LOI), which was used as a proxy for the distribution of organic matter in the sediment, was highest in the top sediment layers with a maximum value of 14.9% measured at monitoring location L04 (L04 right—Figures 2a and 2b). The carbon content (C) in the sediment had a significant positive correlation with LOI (Spearman correlation  $r_s = 0.84$  and  $p = 9.3 \times 10^{-13}$ ). Spatially, both the C content and LOI in the sediment from the deeper monitoring site near the dam (L05) was higher than in the upstream locations closer to the river inflow (L01 and L02, Figure 2d). Furthermore, the PMP was positively correlated with LOI ( $r_s = 0.3$  and  $p = 0.01$ ), nevertheless, no significant correlation was found between PMP and carbon content and PMP and carbon to nitrogen ratio (C:N) in the sediment (Figure S4 in Supporting Information S1).

Dissolved  $\text{CH}_4$  concentration in the pore water slightly increased with increasing depth into the sediment, with the lowest values measured in the top 5 cm (Figure 2c). No consistent longitudinal pattern was observed in porewater dissolved  $\text{CH}_4$  concentration.

The content of free gas in the sediment from the manual sampling ranged from 2.5 to 9.2  $\text{L m}^{-2}$ , with the lowest value found near the reservoir bank in the former riverbed where steeper slopes were found. The data from the manual gas volume sampling and maximum acoustic backscatter were at the upper end of the data reported by Anderson and Martinez (2015). A linear regression, between the logarithm of the gas content and maximum acoustic backscatter including the data from the published study and our own estimates, had a coefficient of determination ( $R^2$ ) of 0.91, which is comparable to the  $R^2 = 0.93$  obtained by Anderson and Martinez (2015) (Figure S3 in Supporting Information S1). By applying the updated calibration curve, spatial maps of gas content in the sediment were obtained for both surveys carried out in the reservoir in 2020 and 2021 (Figures 3a and 3b).

The mapping of gas content in 2020 revealed gas accumulation in locations near to the inner regions of the reservoir bends and coincided with regions of preferred sediment deposition. Comparing the estimated gas content in both surveys, it was found that on average the sediment contained  $1.5 \pm 2.2 \text{ L m}^{-2}$  gas in 2020, whereas in 2021

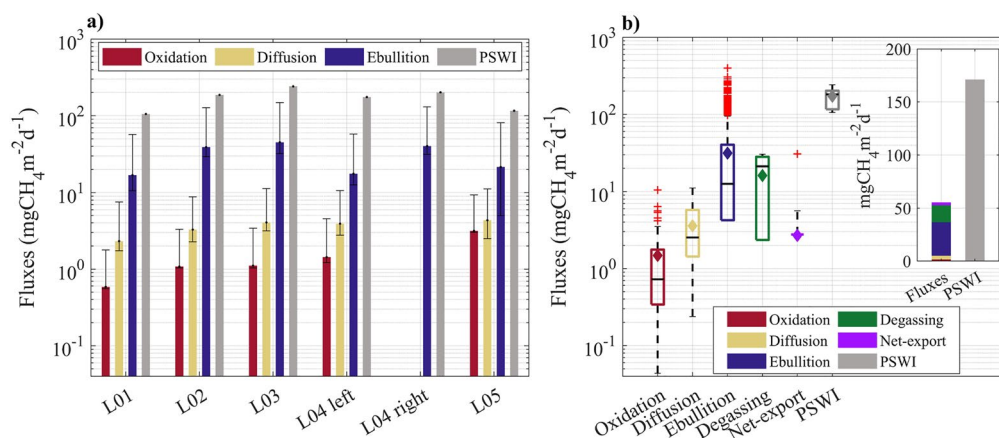


**Figure 4.** (a) Temporal average of different methane fluxes monitored at the sampling sites along the reservoir. PSWI is the potential methane flux at the sediment water interface, calculated as the vertically integrated potential methane production rates and corrected to in situ sediment temperature. Different flux components are shown by different color (see legend) and the vertical error-bars show flux standard deviation. (b) Boxplots of different flux components for the whole reservoir. The horizontal lines inside the boxes are the median values, whereas the mean is showed by the diamond symbol. The upper and lower limits of the boxes represent the 75th and 25th percentiles, respectively. The whiskers show the maximum and minimum values, and the red crosses are outliers. The inset figure with colored bar plot shows the mean fluxes stacked and the gray bar is the average PSWI from the monitoring locations in a linear scale.

for the same area, the estimated gas content was  $5.1 \pm 3.6 \text{ L m}^{-2}$  (see selected areas in Figures 3a and 3b). This represents an average  $\text{CH}_4$  content in free gas of  $1.27 \text{ gCH}_4 \text{ m}^{-2}$  and  $4.42 \text{ gCH}_4 \text{ m}^{-2}$ , respectively, in both years (assuming a  $\text{CH}_4$  fraction of 58% within the free gas). The spatial distribution of sediment gas content differed between both surveys (Figures 3c and 3d). Grid cells with the highest gas content in 2020 did not have the highest gas content in 2021. In particular, the number of cells with high gas content (up to  $10 \text{ L m}^{-2}$ ) increased in 2021, indicating gas storage in the sediment in regions where no or less gas was detected in 2020. Longitudinal and transversal distribution of gas content in the sediment was analyzed based on the more extensive survey conducted in 2020. Longitudinally, the averaged gas content increased towards the dam, and ranged from  $0.7$  to  $5.8 \text{ L m}^{-2}$  (see Figure S5 in Supporting Information S1). In the transversal direction, the gas content was more variable than in the longitudinal direction, especially in the deeper areas, where the gas content ranged from  $1.4$  to  $11.4 \text{ L m}^{-2}$  within a single cross section.

### 3.3. Spatial Variability and Temporal Dynamics of Methane Budget Components

The  $\text{CH}_4$  fraction within gas bubbles sampled during the monitoring period varied from 39% to 94% with a mean value of  $58 \pm 13\%$ , which was then adopted in this study to calculate  $\text{CH}_4$  ebullition fluxes and  $\text{CH}_4$  content in the sediment. Temporally averaged ebullition fluxes were highest at the middle location L03 and lower at the upstream location L01, near to the dam (L05), and at the left side of location L04 (L04 left) (average ebullition in  $\text{mgCH}_4 \text{ m}^{-2} \text{ d}^{-1}$ :  $L01 = 16.9 < L04 \text{ left} = 17.6 < L05 = 21.5 < L02 = 39.2 < L04 \text{ right} = 40.4 < L03 = 45.2$ ). Combining the flux measurements from all monitoring sites (see Figure 4b), the range of ebullition fluxes was from 0 to  $399.8 \text{ mgCH}_4 \text{ m}^{-2} \text{ d}^{-1}$ , with a mean value of  $31.5 \pm 45.3 \text{ mgCH}_4 \text{ m}^{-2} \text{ d}^{-1}$  and a median flux of  $12.6 \text{ mgCH}_4 \text{ m}^{-2} \text{ d}^{-1}$ .

The isotopic analysis showed that  $\text{CH}_4$  in gas bubbles collected near the bottom was consistently more depleted in  $^{13}\text{C}$  (mean  $\delta^{13}\text{C}\text{-CH}_4$  varied from  $-65.1\text{‰}$  to  $-61.5\text{‰}$ ), than in dissolved  $\text{CH}_4$  in surface water ( $-57.5\text{‰}$  to  $-53.8\text{‰}$ ). The resulting mean oxidation fraction ranged from  $0.23 \pm 0.12$  at upstream location L01 to  $0.38 \pm 0.16$  at the deepest location L05 near the dam (Figure S6 in Supporting Information S1). The flux of  $\text{CH}_4$  presumably lost to oxidation (hereafter referred to as the oxidation flux) strongly increased along the reservoir from negligible rates ( $0.6 \text{ mgCH}_4 \text{ m}^{-2} \text{ d}^{-1}$ ) near the inflow (L01), to 5 times higher fluxes ( $3.2 \text{ mgCH}_4 \text{ m}^{-2} \text{ d}^{-1}$ ) near the dam (L05, Figure 4a). No such longitudinal gradient was observed in the diffusive fluxes at the air–water interface. The mean diffusive flux was  $3.6 \pm 2.8 \text{ mgCH}_4 \text{ m}^{-2} \text{ d}^{-1}$ , about two times higher than the oxidation flux ( $1.5 \pm 1.9 \text{ mgCH}_4 \text{ m}^{-2} \text{ d}^{-1}$ ) (Figure 4b). Over the monitored period, both diffusion flux and oxidation flux were higher during the warmer months (Figure S7 in Supporting Information S1).



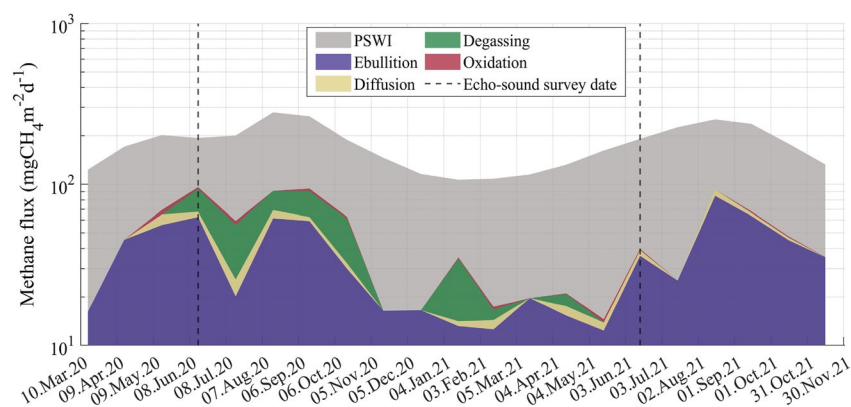


**Figure 5.** Seasonal variations of the measured components of the methane budget with monthly resolution. PSWI is the potential methane flux at the sediment water interface shown as the gray area at the background. Ebullition, diffusion, degassing, and oxidation fluxes are staggered values. The advective fluxes (net export) were for most of the time negative, which indicates to accumulation of  $\text{CH}_4$  in the reservoir or its release to the atmosphere through degassing in the dam. Therefore, the next export of  $\text{CH}_4$  was not included in the staggered values. However, they are shown in Figure S8 in Supporting Information S1. The vertical dashed lines indicate the dates when the echo-sound surveys for the estimation of gas content in the sediment were conducted.

The mean degassing flux at the outflow spillway was  $16.2 \pm 13.1 \text{ mgCH}_4 \text{ m}^{-2} \text{ d}^{-1}$ . The largest fluxes were measured in 2020 during the warmer months from June to October, when the dissolved  $\text{CH}_4$  concentration at the dam was highest (Figure S8 in Supporting Information S1). During May and June 2021, the water level in the main downstream reservoir was above the dam wall due to a flood, and therefore no degassing occurred. After June 2021, degassing measurements could not be continued due to access restrictions at the sampling locations.

The reservoir had a net export flux (difference between inflowing and outflowing dissolved load) ranging from  $-4.3 \text{ mgCH}_4 \text{ m}^{-2} \text{ d}^{-1}$  to  $30.7 \text{ mgCH}_4 \text{ m}^{-2} \text{ d}^{-1}$  (mean value  $2.7 \pm 11.7 \text{ mgCH}_4 \text{ m}^{-2} \text{ d}^{-1}$ , Figure 4b). The downstream export flux was strongly affected by degassing as the dissolved  $\text{CH}_4$  concentration in the outflow was reduced during periods of intensified degassing (Figure S8 in Supporting Information S1). In contrast, when degassing was reduced, the net methane export reached  $30.7 \text{ mgCH}_4 \text{ m}^{-2} \text{ d}^{-1}$ .

The PMP was mostly restricted to the top 20 cm of the sediment (Figure 2a). The vertically integrated production rates (integrated over the top 30 cm layer) provided an estimate of the potential  $\text{CH}_4$  flux at the sediment water interface (PSWI). The variations of mean PSWI among the monitoring locations were similar to those described above for PMP. When extrapolated to the entire reservoir, PSWI was  $\sim 3$  times greater than the sum of the monitored fluxes (ebullition + diffusion + degassing + oxidation + net export), see Figure 4b. When the median fluxes are considered, the difference between the PSWI and the observed methane fluxes increased further (median PSWI  $\sim 5$  times higher than the sum of median fluxes).

In terms of total  $\text{CH}_4$  emissions (ebullition + diffusion + degassing), the reservoir emits on average  $51.3 \text{ mgCH}_4 \text{ m}^{-2} \text{ d}^{-1}$ , in which ebullition had the largest share (61.4%), followed by the degassing (31.6%), and lastly by the diffusive flux (7.0%). However, when the median fluxes are considered, the total  $\text{CH}_4$  fluxes are estimated as  $36.3 \text{ mgCH}_4 \text{ m}^{-2} \text{ d}^{-1}$ , with degassing being the most important flux contributing with 58.4% to the total emissions, followed by ebullition (34.7%), and diffusion (6.9%). One important aspect of the studied reservoir is the presence of the wastewater treatment plant (WTP) with its effluent discharge located upstream of monitoring site L02. From our dataset, it was challenging to isolate any specific impact of the WTP discharge on  $\text{CH}_4$  emissions. Dissolved  $\text{CH}_4$  concentrations, as well as  $\text{CH}_4$  fluxes, carbon and nitrogen content in the sediment, and PMP measured at L02 were not particularly different from the other monitoring sites (see in Figure 4a).

All components of the  $\text{CH}_4$  budgets showed pronounced seasonal variations (Figure 5). The total emissions were lower during the colder months (December to May), which coincides with lower PMP. Over all seasons, PSWI and ebullition fluxes were significantly correlated ( $r_s = 0.8$ ). Similarly, a positive correlation was found between diffusive and ebullition fluxes ( $r_s = 0.7$ , see Figure S9 in Supporting Information S1). For the mean fluxes, degassing was more important than ebullition during periods when ebullition flux was low, for instance in January 2021  $F_{\text{ebul}} 13.2 \text{ mgCH}_4 \text{ m}^{-2} \text{ d}^{-1} < F_{\text{deg}} 20.6 \text{ mgCH}_4 \text{ m}^{-2} \text{ d}^{-1}$ .

**Table 1**  
*Summary of the Environmental Parameters, Measured Methane Fluxes, Estimated Gas Content in the Sediment, and Calculated Ratios Between Gas Content in the Sediment and Relevant CH<sub>4</sub> Fluxes (Representing Turnover Time Scales) for June 2020 and June 2021*

	June 2020	June 2021
Environmental parameters		
Water depth (m)	2.5	3.0
P <sub>atm</sub> (kPa)	98.4 ± 0.7	98.8 ± 0.43
P <sub>hydrostatic</sub> (kPa)	24.5	29.4
Bottom sediment temperature (°C)	12.1 ± 0.4	11.9 ± 0.7
Methane fluxes		
PSWI (mgCH <sub>4</sub> m <sup>-2</sup> d <sup>-1</sup> )	194.1 ± 54.7	191.3 ± 55.4
Ebullition (mgCH <sub>4</sub> m <sup>-2</sup> d <sup>-1</sup> )	62.7 ± 84.9	36.1 ± 49.3
Diffusion (mgCH <sub>4</sub> m <sup>-2</sup> d <sup>-1</sup> )	5.0 ± 2.1	3.0 ± 0.6
Degassing (mgCH <sub>4</sub> m <sup>-2</sup> d <sup>-1</sup> )	26.1	0.0
Net-export (advection) (mgCH <sub>4</sub> m <sup>-2</sup> d <sup>-1</sup> )	-0.9	NA
Oxidation (mgCH <sub>4</sub> m <sup>-2</sup> d <sup>-1</sup> )	2.2 ± 1.9	0.7 ± 0.4
Total Emissions (mgCH <sub>4</sub> m <sup>-2</sup> d <sup>-1</sup> )	93.8	39.1
Free gas in the sediment: echo-sound estimation		
Gas content in the sediment (L m <sup>-2</sup> )	1.5 ± 2.2	5.1 ± 3.6
Methane free gas in the sediment (mgCH <sub>4</sub> m <sup>-2</sup> )	735.9	2561.3
Turnover time		
CH <sub>4</sub> free gas in the sediment/PSWI (d)	3.8	13.4
CH <sub>4</sub> free gas in the sediment/Ebullition (d)	11.7	70.9

*Note.* P<sub>atm</sub> is the mean atmospheric pressure recorded by the weather station installed near the reservoir, P<sub>hydrostatic</sub> is the mean hydrostatic pressure calculated using water depth, PSWI is the potential methane flux at the sediment water interface, and total emissions is the sum of ebullition, degassing, and diffusion CH<sub>4</sub> fluxes. When available we also provide the values' standard deviation. The advective CH<sub>4</sub> flux in 2021 was not measured (NA—Not Available). The italic values indicate the Total Emissions are the sum of methane ebullitive, diffusive, and degassing fluxes.

### 3.4. Methane Budget and CH<sub>4</sub> Storage in the Sediment

We compared the CH<sub>4</sub> budget components for the two months when the acoustic surveys were conducted (June 2020 and June 2021) to the estimated sediment gas content for the reservoir region marked in Figure 3 (detailed information are summarized in Table 1). The estimated gas volume was converted to CH<sub>4</sub> mass using the ideal gas law with the locally measured environmental parameters and assuming a fraction of 58% CH<sub>4</sub>. In June 2020 and 2021, the average CH<sub>4</sub> as free gas in the sediment matrix was 0.7 gCH<sub>4</sub> m<sup>-2</sup> and 2.6 gCH<sub>4</sub> m<sup>-2</sup>.

For both months (June 2020 and June 2021), similar temperatures were recorded; nevertheless in 2021, the water level was 0.5 m higher than in 2020. In terms of the CH<sub>4</sub> budget components, all fluxes were higher in 2020, resulting in higher total CH<sub>4</sub> emissions from the reservoir in that month (93.8 mgCH<sub>4</sub> m<sup>-2</sup> in June 2020 and 39.1 mgCH<sub>4</sub> m<sup>-2</sup> in June 2021).

The ratio of the areal CH<sub>4</sub> content as free gas in the sediment and measured fluxes represent water turnover times that are associated with a recharge of the sediment with newly produced gas (PSWI), or by releasing the stored gas by ebullition. According to these ratios, the free CH<sub>4</sub> gas measured in the sediment matrix represents the cumulative potential CH<sub>4</sub> production of 3.8 and 13.4 days and can support 11.7 and 70.9 days of average ebullition flux in the 2 years, respectively (Table 1).

### 3.5. Temporal Variability of Ebullition

As pointed out above, the ebullition flux was a relevant CH<sub>4</sub> emission pathway in the reservoir, which affects the gas content in the sediment while also being highly variable in time (Figure 4b). High-resolution (daily) mean

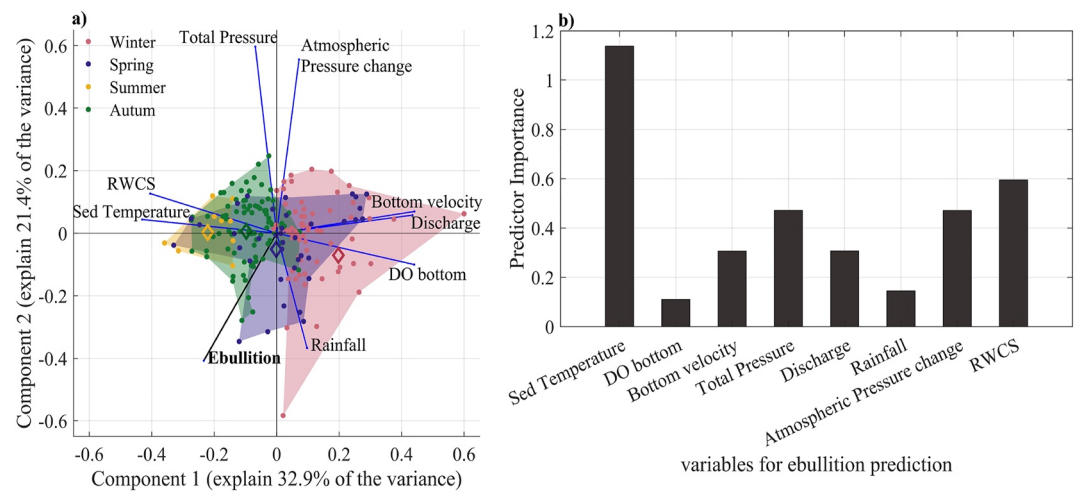


**Figure 6.** (a) Results of a Principal Component Analysis (PCA) with the first two principal components. The dots show daily values, which were seasonally grouped by different colors (see legend) as: winter (December–February), Spring (March–May), Summer (June–August), and Autumn (September–November). (b) Importance of each variable on the prediction of methane ebullition flux from a decision tree model.

values of spatially averaged ebullition fluxes were further analyzed to investigate the main controls on ebullition dynamics. Initially, a correlation matrix with the Spearman rank correlation was calculated for all monitored variables (Figure S10 in Supporting Information S1). Ebullition flux had a significant positive correlation (for a significance level of 5%) with variables related to temperature (water temperature  $r_s = 0.55$ , sediment temperature  $r_s = 0.54$ ) and thermal stratification (RWCS,  $r_s = 0.45$ ). On the other hand, significant negative correlations were observed between ebullition and total pressure at the bottom ( $r_s = -0.49$ ), dissolved oxygen concentration at bottom ( $r_s = -0.36$ ), current speed ( $r_s = -0.20$ ), atmospheric pressure ( $r_s = -0.24$ ), atmospheric pressure change ( $r_s = -0.30$ ), and discharge ( $r_s = -0.22$ ).

A principal component analysis (PCA) was then performed, in which the main aforementioned parameters were considered with the data points seasonally grouped (Figure 6a). Seasonally influenced variables (sediment temperature, bottom velocity, discharge, and dissolved oxygen), mostly contributed to the first PCA component, whereas the pressure related terms (total pressure, atmospheric pressure change, and rainfall) were more aligned with the second principal component. Moreover, the approximate angle of 45° of ebullition with the two principal components suggests that ebullition is affected by both components.

A decision tree classification model was applied to analyze the relative importance of ebullition predictors, in which the input variables were the same as in the PCA. According to the results, the most important predictor for variations in daily mean ebullition rates was sediment temperature, followed by relative water column stability (RWCS), total pressure, and atmospheric pressure change. Dissolved oxygen concentration at the bottom (DO bottom) and rainfall were classified as the least important ebullition predictors (Figure 6b).

Lastly, three statistical models were applied to test whether and how well ebullition variability could be explained by variations in the observed environmental variables presented in Figure 6. A multiple linear regression with log transformed daily ebullition flux resulted in a  $R^2$  of 0.49 and a stepwise linear regression with log transformed daily ebullition flux resulted in a  $R^2$  of 0.47. For the stepwise linear regression, four variables were maintained in the model based on the  $p$ -value (sediment temperature, DO at bottom, total pressure, and atmospheric pressure change). The decision tree model resulted in the best coefficient of determination ( $R^2 = 0.66$ ) between measured and predicted ebullition flux (Figure 7a). The statistical models could well represent the main temporal patterns of the measured ebullition flux, nevertheless, the greater ebullition peaks were underestimated by the models applied (Figure 7b).

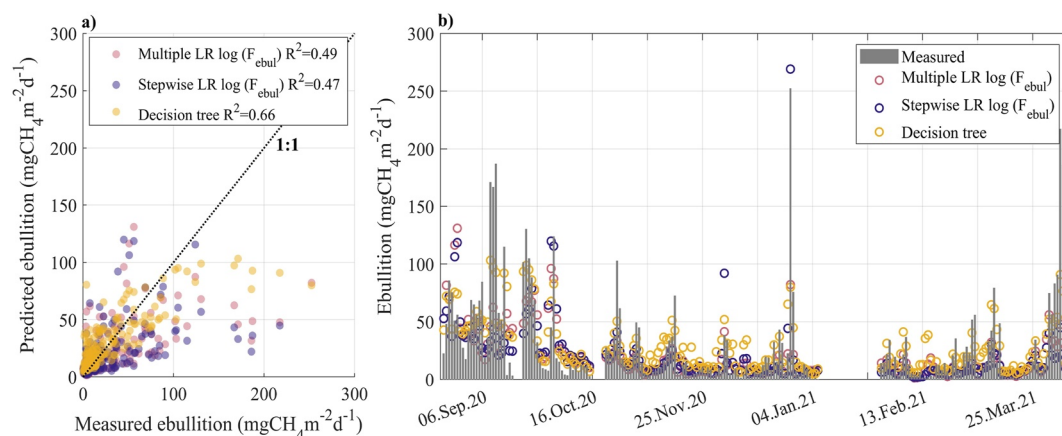


**Figure 7.** (a) Comparison of measured and predicted daily mean ebullition flux for three statistical models indicated by the different color (see legend for model name and coefficient of determination ( $R$ )). The black dotted line shows a 1:1 relationship. (b) Daily fluxes of measured and predicted ebullition fluxes from the three models tested.

## 4. Discussion

### 4.1. Spatial Distribution of Methane in the Sediment

The range of PMP rates in the sediment of the reservoir (up to  $12.8 \text{ mgCH}_4 \text{ L}^{-1} \text{ d}^{-1}$ ) was lower than the range reported for other impoundments in the same region (up to  $25.0 \text{ mgCH}_4 \text{ L}^{-1} \text{ d}^{-1}$  in Wilkinson et al., 2015) and higher than the values reported for a subtropical reservoir in Brazil (up to  $6.0 \text{ mgCH}_4 \text{ L}^{-1} \text{ d}^{-1}$  in Marcon, Sotiri, et al., 2022). The highest PMP rates were measured in the top sediment layers, which had higher organic matter content (LOI). This suggests that methanogenesis in the reservoir was fueled by the supply of fresh organic matter to the sediment surface, as other studies showed that the input of both terrestrial and phytoplankton organic matter enhances  $\text{CH}_4$  production (Berberich et al., 2020; Grasset et al., 2021).

Longitudinal variations in PMP were mainly linked to sediment deposition patterns, as in our shallow system the sediment temperature was nearly homogenous across the monitoring sites. Reservoir geomorphology and sedimentation dynamics are key aspects for methane emission hot-spots in reservoirs (DelSontro et al., 2011; Linkhorst et al., 2021). The narrow-elongated shape of the reservoir with one main inflow led to sediment accumulation in the upstream regions near the inflow and in the regions outside the former river Talweg (mostly in the inner parts of the reservoir bends), which explains the slightly lower PMP at monitoring sites in the old riverbed (L01, L04 left, and L05). The free gas in the sediment estimated from echo-sounder measurements followed similar longitudinal patterns. The higher spatial resolution measurements showed preferred accumulation of free gas in the inner parts of the reservoir bends (Figure 3a).

The mapping of gas content in the sediment also revealed strong temporal heterogeneity. We expected that the amount of free gas in the sediment depends on sediment mechanical properties, and on the sources and sinks of methane (i.e.,  $\text{CH}_4$  production and emission pathways). Temporally, we attribute the variability mainly to the fluxes transporting methane out of the sediment matrix, which is further discussed in a following section.

The average gas content in the sediment ( $1.5 \pm 2.2 \text{ L m}^{-2}$  in 2020 and  $5.1 \pm 3.6 \text{ L m}^{-2}$  in 2021) was in the same range as the average reported for a subtropical reservoir ( $4.4 \text{ L m}^{-2}$  and  $4.6 \text{ L m}^{-2}$  Marcon, Sotiri, et al., 2022). By assuming that the gas content is mainly distributed over the most productive top 30 cm of the sediment, the corresponding volumetric gas fraction were 0.5% and 1.7% in 2020 and 2021 respectively. These fractions are similar to the fraction estimated for Lake Kinneret (<1% and up to 3.8% Katsnelson et al., 2017; Uzhansky et al., 2020), and one order of magnitude smaller than the volumetric gas content reported for different sediment types under laboratory conditions (Liu et al., 2016). Nevertheless, in this study the depth in which the gas voids are distributed could not be derived from our echo-sounder data set, as there is still no well-established direct method. In this way the actual gas fraction may differ, depending on how the gas voids are vertically distributed in the sediment. Other studies reported the depth distribution of gas voids in various depths of the sediment. Dück, Liu, et al. (2019) detected the presence of bubbles starting from 4 cm below the sediment surface in freeze-cores.

Under laboratory conditions, Liu et al. (2018) observed gas voids in sediment depths smaller than 4 cm, which originated from local methane production or vertical migration. For lake Kinneret, Katsnelson et al. (2022) estimated the thickness of the gassy sediment layer to be in the range of 20–40 cm.

We highlight the potential of echo-sounder techniques to remotely access gas distribution in the sediment without disturbing the sediment. Only few studies addressed the gas content in sediment of freshwater ecosystems under in situ conditions. Katsnelson et al. (2017, 2022) determined the gas fraction and the thickness of the gassy sediment layer based on sound velocity, amplitude and frequency analysis of the bottom reflection in lake Kinneret. Anderson and Martinez (2015) proposed a calibration curve for echo-sounder measurements at the 200 kHz frequency, in which the volumetric gas content per unit area is simply estimated based on the maximum backscatter. Our in situ measurements of gas content fitted well to the calibration curve from Anderson and Martinez (2015) and were within the upper region of the calibration curve (Figure S3 in Supporting Information S1), close to the data points from the Hodges Reservoir studied by the authors. This could indicate that both reservoirs have similar sediment properties, but also to the potential of establishing an extensive procedure for measuring in situ sediment gas content in inland waters. The latter is a crucial aspect, as the alternative methods currently available depend on extraction of sediment cores combined with x-ray Computed Tomography (x-ray CT) scanning (Dück, Lorke, et al., 2019), or ground penetrating radar, which is restricted to shallow freshwater (Mustasaar & Comas, 2017).

#### 4.2. Spatial and Temporal Variations of Methane Budget Components

Considering a CH<sub>4</sub> balance for the reservoir we initially hypothesized that the potential methane flux at the sediment water interface (PSWI, which is the vertically integrated PMP) was in the same order as the sum of CH<sub>4</sub> fluxes, including the oxidation flux. Nevertheless, on a monthly basis, the mean PSWI was a factor of 3 (5 for median) greater than all CH<sub>4</sub> sinks to the water column combined (ebullition + diffusion + degassing + oxidation + net export). This is contrasting to the findings from Wilkinson et al. (2015) who found comparable PSWI to the measured ebullition flux in a similarly shallow (4 m water depth) river impoundment.

The sediment cores sampled had a maximum length of 40.5 cm, which is relatively short compared to other studies (e.g., Wilkinson et al., 2015 sampled cores up to 90 cm in length). The shorter length was considered because of lower sedimentation rates in the studied reservoir, which received a mean inflow discharge that is one order of magnitude smaller than in the river impoundments studied by Wilkinson et al. (2015). Nonetheless, it is expected that the deeper sediment layers (beyond 40 cm) would have lower PMP, aligning with the vertical trends observed in our sediment cores (Figure 2a) and supported by findings from other studies (Isidorova et al., 2019; Wilkinson et al., 2015).

We suggest that the gap in the CH<sub>4</sub> budget can be explained by variable sediment gas storage (discussed below), as well as a potential underestimation of CH<sub>4</sub> oxidation rates. In lakes it has been found that 50%–95% of the produced CH<sub>4</sub> can be oxidized in the oxic upper sediment layers (Bastviken, 2009), which is high compared to the oxidized fraction estimated for the reservoir studied here ( $0.8 \pm 0.6\%$ ). For 88% of the monitored period, the DO concentrations near the bottom were higher than 7 mg L<sup>-1</sup> (Figure S1 in Supporting Information S1) and potentially supported a sufficient oxygen flux into the sediment. The sediment-water oxygen fluxes in areas of sediment deposition and intense CH<sub>4</sub> ebullition in an impounded river of comparable water depth have been found to be around 0.5 gO<sub>2</sub> m<sup>-2</sup> d<sup>-1</sup> during low-flow conditions (Lorke et al., 2012). If exclusively used for CH<sub>4</sub> oxidation, this flux can support an oxidation flux of 125 mgCH<sub>4</sub> m<sup>-2</sup> d<sup>-1</sup>, which is in the order of the budget gap ( $111.9 \pm 38.2$  mgCH<sub>4</sub> m<sup>-2</sup> d<sup>-1</sup>). Moreover, the average stable carbon isotopic composition of CH<sub>4</sub> ( $\delta^{13}\text{C-CH}_4$ , see Figure S6 in Supporting Information S1) measured in bubbles collected near the bottom was less depleted in comparison to bottom waters of lakes in Sweden (down to  $-80.6\%$  Bastviken et al., 2002) and in gas bubbles from bottom sediments in arctic lakes (down to  $-79.7\%$  Walter et al., 2008). The comparably low depletion found in bubbles at our study sites suggest that CH<sub>4</sub> oxidation in the sediment has caused a change in  $\delta^{13}\text{C-CH}_4$  in gas bubbles, as oxidation of CH<sub>4</sub> leads to an increase in the  $\delta^{13}\text{C-CH}_4$  signature (Bastviken et al., 2002; Sawakuchi et al., 2016). These oxidative losses were not accounted for in the oxidation rates estimated from the difference of  $\delta^{13}\text{C-CH}_4$  in bubbles and at the water surface and may have caused severe underestimation of the oxidation fluxes. Additionally, the data gaps or limitations in the temporal-spatial resolution of sampling may have affected the flux estimates by not capturing hot moments of ebullition, diffusion, or degassing emissions. However, we also acknowledged that uncertainties in the estimated PMP and fluxes might have contributed to the imbalance in the CH<sub>4</sub> budget.

Consistent longitudinal gradients were detected in diffusive and oxidation  $\text{CH}_4$  fluxes, in which both increased toward the dam (Figure 4a and Figure S7 in Supporting Information S1), probably due to the accumulation of dissolved  $\text{CH}_4$  in the water along the reservoir. In contrast,  $\text{CH}_4$  ebullition was larger at the monitoring sites located at the mid-stretch of the reservoir (from sites L02 to L04) where higher PSWI was also detected (significant correlation found,  $r_s = 0.79$ , between Ebullition and PSWI, Figure S9 in Supporting Information S1). The effect of the wastewater treatment plant (WTP) discharge on  $\text{CH}_4$  fluxes could not be disentangled from the general longitudinal trends. Nevertheless, we cannot exclude the possibility that WTP discharge influences  $\text{CH}_4$  dynamics in water bodies. In smaller streams, Alshboul et al. (2016) observed increased dissolved  $\text{CH}_4$  concentrations from effluent discharge, in which the  $\text{CH}_4$  concentration had a linear dependence on the organic load of the wastewater.

Unfortunately, due to depth restrictions for the deployment of bubble traps, ebullition could not be measured at the shallow (water depth  $<1.0$  m) upstream regions of the reservoir, and therefore, these regions had to be excluded from the  $\text{CH}_4$  budget. Temporal variability was found in all measured  $\text{CH}_4$  budget components. The largest fluxes were recorded during the warmer months, which is explained by the exponential dependence of  $\text{CH}_4$  production on temperature (Aben et al., 2017; Wilkinson et al., 2019). The high frequency variation of ebullition flux is analyzed below.

Taking into account the  $\text{CH}_4$  budget for the entire reservoir, represented on Figure 4b, the total  $\text{CH}_4$  emissions (ebullition + diffusion + degassing) of the reservoir ( $51.3 \text{ mgCH}_4 \text{ m}^{-2} \text{ d}^{-1}$  mean fluxes and  $36.3 \text{ mgCH}_4 \text{ m}^{-2} \text{ d}^{-1}$  median fluxes) was 3–5 times lower than the average areal emissions reported for reservoirs worldwide (Deemer et al., 2016; Rosentreter et al., 2021). In our study, ebullition and degassing had the main share accounting for 93% of the total  $\text{CH}_4$  emissions, contributing respectively to 61.4% (34.7% median fluxes) and 31.6% (58.4% median fluxes). Both degassing and ebullition fluxes are variable across different reservoirs. Median degassing flux was reported as one order magnitude lower than ebullition flux (Deemer et al., 2016); however, a modeling approach showed that for stratified hydropower reservoirs the degassing can be up to four times higher than ebullition (Delwiche et al., 2022). Temporally, considering monthly fluxes, the share of ebullition and degassing to the total  $\text{CH}_4$  emissions was variable. In July 2020 and January 2021, when there was a reduction of ebullition, degassing was the dominant  $\text{CH}_4$  emission pathway.

### 4.3. Linking Methane Budget Components to Gas Storage in the Sediment

To the best of our knowledge, this is the first time that temporal variability of in situ gas content in the sediment was linked to the  $\text{CH}_4$  balance in an aquatic ecosystem. The average gas content in the sediment was remarkably different between both surveys (by a factor of  $\sim 3.5$  between 2020 and 2021). Differences in sediment temperature between both years could not explain the change ( $0.2^\circ\text{C}$  between the years). We hypothesize that the dynamics in processes removing  $\text{CH}_4$  from the reservoir (ebullition + diffusion + oxidation + degassing) lead to a reduction of free gas in the sediment matrix. Consequently, the gas storage in the sediment increases when the efflux of  $\text{CH}_4$  is diminished (see Figure 5 and Table 1 for contrasting  $\text{CH}_4$  fluxes for the two periods when gas content in the sediment was estimated).

The ratio between estimated gas content in the sediment and the PSWI revealed that the sediment had stored an amount of  $\text{CH}_4$  potentially produced in  $\sim 4$  days in June 2020 up to 13 days in June 2021. The gas stored in the sediment for both periods (June 2020 and June 2021), represented 12–71 days of averaged ebullition flux respectively, and therefore, even without production, the sediment could potentially supply gas for the mean ebullition flux of more than two months.

The gas storage in the sediment matrix (such as found in June 2021), suggests that temporarily reduced  $\text{CH}_4$  fluxes do not necessarily decrease the reservoir's potential contribution to the  $\text{CH}_4$  emissions, as the stored gas can later be released to the water column, depending on external triggers. The gas retention capacity of the sediment matrix can affect the  $\text{CH}_4$  balance by affecting oxidation and diffusion, which in turn can impact the  $\text{CH}_4$  content in the bubbles leaving the sediment, the sediment mechanical properties (Sills et al., 1991; Wheeler, 1988), and the timing of ebullition events. Our findings suggest that the gas storage in the sediment was connected to the  $\text{CH}_4$  fluxes from the reservoir, emphasizing its significance as a component of the  $\text{CH}_4$  budget and a potential contributor to the observed mismatch in the balance of production and emission rates (Table 1). Moreover, it may mask the dependence of ebullition on the environmental variables, which are discussed in the following section.

We suggest that gas storage in the sediment should be considered in modeling approaches of CH<sub>4</sub> dynamics and emissions from lakes and reservoirs, similar to ebullition models for terrestrial wetlands (Ma et al., 2022; Peltola et al., 2018). Sediment gas storage can be described as a buffer with a maximum holdup capacity for gas, which is recharged by production and depleted by various outflows (i.e., ebullition, diffusion, and oxidation). In turn, it is controlled by sediment properties such as grain size distribution (Jain & Juanes, 2009; Liu et al., 2016), sediment bulk density and fracture toughness (Katsman, 2015), and environmental conditions of temperature and pressure. Peltola et al. (2018) tested different model approaches for estimating CH<sub>4</sub> ebullition from boreal wetlands and showed that adding a volume threshold for gas in the sediment led to improved simulation results of ebullition fluxes.

In our study, the areal gas content was converted to a volumetric content based on the depth of PMP. In a recent study Katsnelson et al. (2022) proposed a method to determine the thickness of the gassy layer of the sediment from measurements combining a sound transducer and a hydrophone with sound pulses in the frequency range of 0.3–3.5 kHz. Nevertheless, obtaining in situ vertical distribution of gassy sediment layers is still an open issue.

#### 4.4. Controls on Methane Ebullition and Temporal Dynamics

Since ebullition flux serves as the primary pathway for CH<sub>4</sub> outflow from the sediment, it directly affects the dynamics of gas storage in the sediment. The quasi-continuous time-series of ebullition rates measured by automatic bubble traps were used to analyze the drivers of their temporal variations. Principal component analysis (PCA) showed that the drivers of ebullition fluxes can be classified into two groups: one related to temperature and another linked to pressure. While the sediment temperature enhances ebullition flux due to its relationship to methane production (Aben et al., 2017; Wilkinson et al., 2019), the decrease in pressure at the sediment water interface can trigger bubble release from the sediment, such pressure reductions can be due to water level oscillations (Maeck et al., 2014) or atmospheric pressure variations (Marcon et al., 2019; Natchimuthu et al., 2016). The significance of sediment temperature, relative water column stability (RWCS), total pressure, and pressure change in explaining the temporal variability of ebullition was further confirmed by a decision tree model. These parameters were found to be most important for explaining the observed variability of ebullition compared to the other environmental variables.

We observed intensified ebullition during periods of more stable density stratification (higher RWCS). Density stratification attenuates the vertical transport and the exchange of gases and substances through the water column (Guseva et al., 2020; Vachon et al., 2019). The increased CH<sub>4</sub> concentration in the water column leads to a reduction of CH<sub>4</sub> diffusion from the sediment (Langenegger et al., 2019) and increased oxidation rates (Vachon et al., 2019; Zimmermann et al., 2021). In the case of the pre-dam, the RWCS was controlled by temperature, but also affected by the inflow discharge (see Figure S10 in Supporting Information S1—RWCS was negatively correlated to discharge). Higher discharge from the inflow river led to an increase in the current velocity, which contributes to water column mixing.

The tested regressions and decision tree models could explain 47%–66% of ebullition variability with a better performance of the decision tree model (Figure 7a). This better performance of the decision tree can be mostly attributed to the model's capability of considering non-linear relationships between the variables. Using a multiple regression model, DelSontro et al. (2016) explained 52% of ebullition variability from different ponds and lakes based on sediment temperature and total phosphorous. Whereas for a larger data set of different reservoirs, Prairie et al. (2021) predicted ebullition flux as a function of reservoir littoral area and global horizontal radiance explaining 26% of its variability. Our results suggest that the inclusion of other parameters such as atmospheric pressure and water column stability can improve the prediction of ebullition even further.

## 5. Conclusions

Based on extensive field monitoring, we analyzed the CH<sub>4</sub> budget of a small and shallow temperate reservoir. From the vertical profiles of PMP and LOI, we showed that the top organic matter rich sediment layers had the greatest PMP. A large gap between potential methane fluxes at the sediment water interface (PSWI) and measured fluxes was identified, which could be caused by a combination of factors including sediment gas storage and the underestimated CH<sub>4</sub> oxidation in the sediment.

Longitudinally, diffusive and oxidation CH<sub>4</sub> fluxes strongly increased towards the dam, whereas ebullition was larger at the mid-stretch of the reservoir at locations with higher PMP. Considering the total CH<sub>4</sub> emissions

from the reservoir, ebullition and degassing accounted for 93% of the emissions. The relative share of each flux to the emissions varied with time. The combination of different data analysis methods confirmed the complex nature of ebullition and its dependence on several parameters. Sediment temperature, total pressure (hydrostatic + atmospheric), atmospheric pressure change, relative water column stability, and bottom velocity were the main controlling factors for the temporal variations in daily ebullition rates. The combination of environmental parameters in a decision tree model explained 66% of ebullition variability.

The gas content in the sediment could be estimated from an acoustically derived parameter (maximum backscatter), in which a previously reported empirical relationship was validated and adopted. Gas accumulation of up to 15 L m<sup>-2</sup> were observed in regions of preferred sediment deposition. The temporal variability of gas content in the sediment could be linked to the monitored methane budget components, in which periods of intensified emissions resulted in depletion of the gas stored in the sediment. Nonetheless, when emissions are damped, the sediment matrix can store the cumulative CH<sub>4</sub> production of several days, which in turn can maintain mean ebullition fluxes over months. We discussed the possible effect of sediment gas storage on the CH<sub>4</sub> budget in the shallow lakes and reservoirs and we suggest that its implementation in process-based model can improve predictions of CH<sub>4</sub> emissions from these aquatic ecosystems.

In addition, we confirmed the potential of echo-sounding to access the gas content in the sediment matrix, which contributes to the understanding of methane spatial variability and its temporal dynamics in inland waters. However, further investigations and calibrations are still necessary for the application of the echo-sounder for different systems and for describing the vertical distribution of gas voids in the sediment matrix.

### Data Availability Statement

The data sets of in situ methane fluxes measurements, time series of daily ebullition flux and mean environmental variables, laboratorial analysis of PMP, dissolved CH<sub>4</sub> concentration in porewater, LOI, carbon and nitrogen content of sediment samples, and gas content in the sediment for the spatial grid of the reservoir used in this study are provided on the repository Zenodo (<https://doi.org/10.5281/zenodo.8119001>) (Marcon, Schwarz, et al., 2022).

### Acknowledgments

We would like to thank the reservoir operator Wuppertalverband for the cooperation and support during the monitoring program. We kindly thank Christoph Bors, Mario Axler, and Leonard Martin Kaufhold for their help and support during field and laboratory work. The study was financially supported by the German Federal Environmental Foundation (DBU—Deutsche Bundesstiftung Umwelt, Grant AZ 34765-01 and AZ 37831-01) and by the German Research Foundation (DFG, Grant LO 1150/16). Open Access funding enabled and organized by Projekt DEAL.

### References

- Aben, R. C. H., Barros, N., Van Donk, E., Frenken, T., Hilt, S., Kazanjian, G., et al. (2017). Cross continental increase in methane ebullition under climate change. *Nature Communications*, 8(1), 1–8. <https://doi.org/10.1038/s41467-017-01535-y>
- Alshboul, Z., Encinas-Fernández, J., Hofmann, H., & Lorke, A. (2016). Export of dissolved methane and carbon dioxide with effluents from municipal wastewater treatment plants. *Environmental Science and Technology*, 50(11), 5555–5563. <https://doi.org/10.1021/acs.est.5b04923>
- Anderson, M. A., & Martinez, D. (2015). Methane gas in lake bottom sediments quantified using acoustic backscatter strength. *Journal of Soils and Sediments*, 15(5), 1246–1255. <https://doi.org/10.1007/s11368-015-1099-1>
- Bastviken, D. (2009). Methane. In *Encyclopedia of Inland Waters* (pp. 783–805). Elsevier. <https://doi.org/10.1016/b978-0-12370626-3.00117-4>
- Bastviken, D., Cole, J., Pace, M., & Tranvik, L. (2004). Methane emissions from lakes: Dependence of lake characteristics, two regional assessments, and a global estimate. *Global Biogeochemical Cycles*, 18(4), 1–12. <https://doi.org/10.1029/2004GB002238>
- Bastviken, D., Ejlertsson, J., & Tranvik, L. (2002). Measurement of methane oxidation in lakes: A comparison of methods. *Environmental Science and Technology*, 36(15), 3354–3361. <https://doi.org/10.1021/es10311p>
- Berberich, M. E., Beaulieu, J. J., Hamilton, T. L., Waldo, S., & Buffam, I. (2020). Spatial variability of sediment methane production and methanogen communities within a eutrophic reservoir: Importance of organic matter source and quantity. *Limnology & Oceanography*, 65(6), 1336–1358. <https://doi.org/10.1002/lno.11392>
- Branco, C. W. C., Kozłowsky-Suzuki, B., Sousa-Filho, I. F., Guarino, A. W. S., & Rocha, R. J. (2009). Impact of climate on the vertical water column structure of Lajes reservoir (Brazil): A tropical reservoir case. *Lakes and Reservoirs: Research and Management*, 14(3), 175–191. <https://doi.org/10.1111/j.1440-1770.2009.00403.x>
- Deemer, B. R., Harrison, J. A., Li, S., Beaulieu, J. J., Delsontro, T., Barros, N., et al. (2016). Greenhouse gas emissions from reservoir water surfaces: A new global synthesis manuscript. *BioScience*, 66(11), 949–964. <https://doi.org/10.1093/biosci/biw117>
- DelSontro, T. S., Boutet, L., St-Pierre, A., del Giorgio, P. A., & Prairie, Y. T. (2016). Methane ebullition and diffusion from northern ponds and lakes regulated by the interaction between temperature and system productivity. *Limnology & Oceanography*, 61(S1), S62–S77. <https://doi.org/10.1002/lno.10335>
- DelSontro, T. S., Kunz, M. J., Kempter, T., Wüest, A., Wehrli, B., & Senn, D. B. (2011). Spatial heterogeneity of methane ebullition in a large tropical reservoir. *Environmental Science and Technology*, 45(23), 9866–9873. <https://doi.org/10.1021/es2005545>
- Delwiche, K. B., Harrison, J. A., Maasakkers, J. D., Sulprizio, M. P., Worden, J., Jacob, D. J., & Sunderland, E. M. (2022). Estimating driver and pathways for hydroelectric reservoir methane emissions using a new mechanistic model. *Journal of Geophysical Research: Biogeosciences*, 127(8), 1–24. <https://doi.org/10.1029/2022jg006908>
- Dück, Y., Liu, L., Lorke, A., Ostrovsky, I., Katsman, R., & Jokiel, C. (2019). A novel freeze corer for characterization of methane bubbles and assessment of coring disturbances. *Limnology and Oceanography: Methods*, 17(5), 305–319. <https://doi.org/10.1002/lom3.10315>
- Dück, Y., Lorke, A., Jokiel, C., & Gierse, J. (2019). Laboratory and field investigations on freeze and gravity core sampling and assessment of coring disturbances with implications on gas bubble characterization. *Limnology and Oceanography: Methods*, 17(11), 585–606. <https://doi.org/10.1002/lom3.10335>



- Fischer, H. B., List, E. J., Koh, R. C. Y., Imberger, J., & Brooks, N. H. (1979). *Mixing in inland and coastal waters*. Academic Press Inc.
- Gerardo-Nieto, O., Astorga-España, M. S., Mansilla, A., & Thalasso, F. (2017). Initial report on methane and carbon dioxide emission dynamics from sub-Antarctic freshwater ecosystems: A seasonal study of a lake and a reservoir. *Science of the Total Environment*, 593, 144–154. <https://doi.org/10.1016/j.scitotenv.2017.02.144>
- Goldenfum, J. A. (2010). *GHG measurement guidelines for freshwater reservoirs* (In J. A. Goldenfum (Ed.), Ed.). The International Hydropower Association (IHA).
- Grasset, C., Moras, S., Isidorova, A., Couture, R., Linkhorst, A., & Sobek, S. (2021). An empirical model to predict methane production in inland water sediment from particular organic matter supply and reactivity. *Limnology and Oceanography, Middelburg 1989*, 66(10), 1–13. <https://doi.org/10.1002/lno.11905>
- Guseva, S., Bleninger, T., Jöhnk, K., Polli, B. A., Tan, Z., Thiery, W., et al. (2020). Multimodel simulation of vertical gas transfer in a temperate lake. *Hydrology and Earth System Sciences*, 24(2), 697–715. <https://doi.org/10.5194/hess-24-697-2020>
- Hilgert, S., Fernandes, C. V. S., & Fuchs, S. (2019). Redistribution of methane emission hot spots under drawdown conditions. *Science of the Total Environment*, 646, 958–971. <https://doi.org/10.1016/j.scitotenv.2018.07.338>
- IPCC. (2021). *Climate change 2021: The physical science basis. Contribution of Working group I to the Sixth assessment Report of the Intergovernmental Panel on Climate change* (In V. Masson-Delmotte, P. Zhai, A. Pirani, S. L. Connors, C. Péan (Eds.), et al., Eds.). Cambridge University Press. <https://doi.org/10.1017/9781009157896>
- Isidorova, A., Grasset, C., Mendonça, R., & Sobek, S. (2019). Methane formation in tropical reservoirs predicted from sediment age and nitrogen. *Scientific Reports*, 9(1), 1–9. <https://doi.org/10.1038/s41598-019-47346-7>
- Jain, A. K., & Juanes, R. (2009). Preferential mode of gas invasion in sediments: Grain-scale mechanistic model of coupled multiphase fluid flow and sediment mechanics. *Journal of Geophysical Research*, 114(8), 1–19. <https://doi.org/10.1029/2008JB006002>
- Katsman, R. (2015). Correlation of shape and size of methane bubbles in fine-grained muddy aquatic sediments with sediment fracture toughness. *Journal of Structural Geology*, 70, 56–64. <https://doi.org/10.1016/j.jsg.2014.11.002>
- Katsnelson, B., Katsman, R., Lunkov, A., & Ostrovsky, I. (2017). Acoustical methodology for determination of gas content in aquatic sediments, with application to Lake Kinneret, Israel, as a case study. *Limnology and Oceanography: Methods*, 15(6), 531–541. <https://doi.org/10.1002/lom3.10178>
- Katsnelson, B., Uzhansky, E., Lunkov, A., & Ostrovsky, I. (2022). Characterization of the gassy sediment layer in shallow water using an acoustical method: Lake Kinneret as a case study. *Limnology and Oceanography: Methods*, 20(9), 581–593. <https://doi.org/10.1002/lom3.10506>
- Langenegger, T., Vachon, D., Donis, D., & McGinnis, D. F. (2019). What the bubble knows: Lake methane dynamics revealed by sediment gas bubble composition. *Limnology and Oceanography, February*, 64(4), 1526–1544. <https://doi.org/10.1002/lno.11133>
- Linkhorst, A., Paranaíba, J. R., Mendonça, R., Rudberg, D., DelSontro, T., Barros, N., & Sobek, S. (2021). Spatially resolved measurements in tropical reservoirs reveal elevated methane ebullition at river inflows and at high productivity. *Global Biogeochemical Cycles*, 35(5), 1–16. <https://doi.org/10.1029/2020GB006717>
- Liss, P. S., & Slater, P. G. (1974). Flux of gases across the Air-Sea interface. *Nature*, 247(5438), 181–184. <https://doi.org/10.1038/247181a0>
- Liu, L., De Kock, T., Wilkinson, J., Cnudde, V., Xiao, S., Buchmann, C., et al. (2018). Methane bubble growth and migration in aquatic sediments observed by X-ray  $\mu$ CT. *Environmental Science and Technology*, 52(4), 2007–2015. <https://doi.org/10.1021/acs.est.7b06061>
- Liu, L., Sotiri, K., Dück, Y., Hilgert, S., Ostrovsky, I., Uzhansky, E., et al. (2019). The control of sediment gas accumulation on spatial distribution of ebullition in Lake Kinneret. *Geo-Marine Letters*, 40(4), 453–466. <https://doi.org/10.1007/s00367-019-00612-z>
- Liu, L., Wilkinson, J., Koca, K., Buchmann, C., & Lorke, A. (2016). The role of sediment structure in gas bubble storage and release. *Journal of Geophysical Research: Biogeosciences, August*(7), 1–14. <https://doi.org/10.1002/2016JG003456>
- Lorke, A., McGinnis, D. F., Maeck, A., & Fischer, H. (2012). Effect of ship locking on sediment oxygen uptake in impounded rivers. *Water Resources Research*, 48(12), 1–7. <https://doi.org/10.1029/2012WR012483>
- Ma, S., Jiang, L., Wilson, R. M., Chanton, J. P., Bridgman, S., Niu, S., et al. (2022). Evaluating alternative ebullition models for predicting peatland methane emission and its pathways via data–model fusion. *Biogeosciences*, 19(8), 2245–2262. <https://doi.org/10.5194/bg-19-2245-2022>
- Maa vara, T., Chen, Q., Van Meter, K., Brown, L. E., Zhang, J., Ni, J., & Zarfl, C. (2020). River dam impacts on biogeochemical cycling. *Nature Reviews Earth & Environment*, 1(2), 103–116. <https://doi.org/10.1038/s43017-019-0019-0>
- Maa vara, T., Lauerwald, R., Regnier, P., & Van Cappellen, P. (2017). Global perturbation of organic carbon cycling by river damming. *Nature Communications*, 8(May), 1–10. <https://doi.org/10.1038/ncomms15347>
- Maeck, A., Del Sontro, T. S., McGinnis, D. F., Fischer, H., Flury, S., Schmidt, M., et al. (2013). Sediment trapping by dams creates methane emission hot spots. *Environmental Science and Technology*, 47(15), 8130–8137. <https://doi.org/10.1021/es4003907>
- Maeck, A., Hofmann, H., & Lorke, A. (2014). Pumping methane out of aquatic sediments - Ebullition forcing mechanisms in an impounded river. *Biogeosciences*, 11(11), 2925–2938. <https://doi.org/10.5194/bg-11-2925-2014>
- Marcon, L., Bleninger, T., Männich, M., & Hilgert, S. (2019). High-frequency measurements of gas ebullition in a Brazilian subtropical reservoir—Identification of relevant triggers and seasonal patterns. *Environmental Monitoring and Assessment*, 191(6), 357. <https://doi.org/10.1007/s10661-019-7498-9>
- Marcon, L., Schwarz, M., Backes, L., Offermann, M., Schreiber, F., Hilgert, S., et al. (2022). Date set for the manuscript: The role of sediment gas storage in the methane dynamics of a shallow freshwater reservoir (version 2.0) [Dataset]. Zenodo. <https://doi.org/10.5281/zenodo.8119001>
- Marcon, L., Sotiri, K., Bleninger, T., Lorke, A., Männich, M., & Hilgert, S. (2022). Acoustic mapping of gas stored in sediments of shallow aquatic systems linked to methane production and ebullition patterns. *Frontiers in Environmental Science*, 10(April), 1–17. <https://doi.org/10.3389/fenvs.2022.876540>
- Martinez, D., & Anderson, M. A. (2013). Methane production and ebullition in a shallow, artificially aerated, eutrophic temperate lake (Lake Elsinore, CA). *Science of the Total Environment*, 454–455, 457–465. <https://doi.org/10.1016/j.scitotenv.2013.03.040>
- Morris, G. (2020). Classification of management alternatives to Combat reservoir sedimentation. *Water*, 12(3), 861. <https://doi.org/10.3390/w12030861>
- Mustasaar, M., & Comas, X. (2017). Spatiotemporal variability in biogenic gas dynamics in a subtropical peat soil at the laboratory scale is revealed using high-resolution ground-penetrating radar. *Journal of Geophysical Research: Biogeosciences*, 122(9), 2219–2232. <https://doi.org/10.1002/2016JG003714>
- Natchimuthu, S., Sundgren, I., Galfalk, M., Klemetsson, L., Crill, P., Danielsson, A., & Bastviken, D. (2016). Spatio-temporal variability of lake CH<sub>4</sub> fluxes and its influence on annual whole lake emission estimates. *Limnology & Oceanography*, 61(S1), S13–S26. <https://doi.org/10.1002/lno.10222>
- Paul, L. (2003). Nutrient elimination in pre-dams: Results of long term studies. *Hydrobiologia*, 504(1–3), 289–295. <https://doi.org/10.1023/B:HYDR.0000008528.34920.b2>

- Peltola, O., Raivonen, M., Li, X., & Vesala, T. (2018). Technical note: Comparison of methane ebullition modelling approaches used in terrestrial wetland models. *Biogeosciences*, *15*(3), 937–951. <https://doi.org/10.5194/bg-15-937-2018>
- Prairie, Y. T., Mercier-Blais, S., Harrison, J. A., Soued, C., del Giorgio, P., Harby, A., et al. (2021). A new modelling framework to assess biogenic GHG emissions from reservoirs: The G-res tool. *Environmental Modelling & Software*, *143*, 105117. <https://doi.org/10.1016/j.envsoft.2021.105117>
- Rosentreter, J. A., Borges, A. V., Deemer, B. R., Holgerson, M. A., Liu, S., Song, C., et al. (2021). Half of global methane emissions come from highly variable aquatic ecosystem sources. *Nature Geoscience*, *14*(April), 225–230. <https://doi.org/10.1038/s41561-021-00715-2>
- Saunio, M., Stavert, A. R., Poulter, B., Bousquet, P., Canadell, J. G., Jackson, R. B., et al. (2020). The global methane budget 2000–2017. *Earth System Science Data*, *12*(3), 1561–1623. <https://doi.org/10.5194/essd-12-1561-2020>
- Sawakuchi, H. O., Bastviken, D., Sawakuchi, A. O., Ward, N. D., Borges, C. D., Tsai, S. M., et al. (2016). Oxidative mitigation of aquatic methane emissions in large Amazonian rivers. *Global Change Biology*, *22*(3), 1075–1085. <https://doi.org/10.1111/gcb.13169>
- Sills, G. C., Thomas, S. D., Gardner, T. N., & Wheeler, S. J. (1991). Behaviour of offshore soils containing gas bubbles. *Géotechnique*, *41*(2), 227–241. <https://doi.org/10.1680/geot.1991.41.2.227>
- Smith, K. A. A., Ball, T., Conen, F., Dobbie, K. E. E., Massheder, J., & Rey, A. (2003). Exchange of greenhouse gases between soil and atmosphere: Interactions of soil physical factors and biological processes. *European Journal of Soil Science*, *54*(December), 779–791. <https://doi.org/10.1046/j.1365-2389.2003.00567.x>
- Uzhansky, E., Katsnelson, B., Lunkov, A., & Ostrovsky, I. (2020). Spatial and temporal variability of free gas content in shallow sediments: Lake Kinneret as a case study. *Geo-Marine Letters*, *40*(4), 491–505. <https://doi.org/10.1007/s00367-019-00629-4>
- Vachon, D., Langenegger, T., Donis, D., & McGinnis, D. F. (2019). Influence of water column stratification and mixing patterns on the fate of methane produced in deep sediments of a small eutrophic lake. *Limnology & Oceanography*, *1*(5), 2114–2128. <https://doi.org/10.1002/lno.11172>
- Walter, K. M., Chanton, J. P., Chapin, F. S., Schuur, E. A. G., & Zimov, S. A. (2008). Methane production and bubble emissions from arctic lakes: Isotopic implications for source pathways and ages. *Journal of Geophysical Research*, *113*(3), G00A08. <https://doi.org/10.1029/2007JG000569>
- Welch, E. B., & Naczk, F. (1992). *Ecological effects of waste water*. 2nd ed. CRC Press. <https://doi.org/10.4324/9780203038499>
- Wetzel, R. G. (2001). *Limnology: Lake and river ecosystems*. 3rd ed. Academic Press Inc.
- Wheeler, S. J. (1988). The undrained shear strength of soils containing large gas bubbles. *Geotechnique*, *3*, 399–413. <https://doi.org/10.1680/geot.1988.38.3.399>
- Wilkinson, J., Bodmer, P., & Lorke, A. (2019). Methane dynamics and thermal response in impoundments of the Rhine River, Germany. *Science of the Total Environment*, *659*, 1045–1057. <https://doi.org/10.1016/j.scitotenv.2018.12.424>
- Wilkinson, J., Bors, C., Burgis, F., Lorke, A., & Bodmer, P. (2018). Measuring CO<sub>2</sub> and CH<sub>4</sub> with a portable gas analyzer: Closed-loop operation, optimization and assessment. *PLoS One*, *13*(4), 1–16. <https://doi.org/10.1371/journal.pone.0193973>
- Wilkinson, J., Maeck, A., Alshboul, Z., & Lorke, A. (2015). Continuous Seasonal River Ebullition measurements linked to sediment methane formation. *Environmental Science and Technology*, *49*(22), 13121–13129. <https://doi.org/10.1021/acs.est.5b01525>
- Zimmermann, M., Mayr, M. J., Bürgmann, H., Eugster, W., Steinsberger, T., Wehrli, B., et al. (2021). Microbial methane oxidation efficiency and robustness during lake overturn. *Limnology and Oceanography Letters*, *6*(6), 320–328. <https://doi.org/10.1002/lol2.10209>

## References From the Supporting Information

- Bossard, V. P., Joller, T., & Szabo, E. (1981). Die quantitative Erfassung von Methan im Seewasser. *Birkhäuser Verlag Basel*, *43*(1), 200–211. <https://doi.org/10.1007/bf02502482>
- Crusius, J., & Wanninkhof, R. (2003). Gas transfer velocities measured at low wind speed over a lake. *Limnology & Oceanography*, *48*(3), 1010–1017. <https://doi.org/10.4319/lo.2003.48.3.1010>
- Delwiche, K., & Hemond, H. F. (2017). An enhanced bubble size sensor for long-term ebullition studies. *Limnology and Oceanography: Methods*, *15*(10), 821–835. <https://doi.org/10.1002/lom3.10201>
- Delwiche, K., Senft-Grupp, S., & Hemond, H. (2015). A novel optical sensor designed to measure methane bubble sizes in situ. *Limnology and Oceanography: Methods*, *13*(12), 712–721. <https://doi.org/10.1002/lom3.10060>
- Heiri, O., Lotter, A. F., & Lemcke, G. (2001). Loss on ignition as a method for estimating organic and carbonate content in sediments: Reproducibility and comparability of results. *Journal of Paleolimnology*, *25*(December), 101–110. <https://doi.org/10.1023/A>
- Wanninkhof, R. (2014). Relationship between wind speed and gas exchange over the ocean revisited. *Limnology and Oceanography: Methods*, *12*(JUN), 351–362. <https://doi.org/10.4319/lom.2014.12.351>